al forms. Proc. IEEE 69 (6), 676–696.
for Physicists. Cambridge University

tics. IEEE Press, John Wiley & Sons,

etism. Dover Publications, New York
edition of 1891), 506 pp.
tation. Freeman, San Francisco, 1279

d Regularization Problems. Elsevier,

eory and Methods. Elsevier, 856 pp.

CHAPTER 18

3D Electromagnetic Holographic Imaging in Active Monitoring of Sea-Bottom Geoelectrical Structures

Michael S. Zhdanov[a], Martin Cuma[b], *and* Takumi Ueda[c]

Contents

1. Introduction

During the last few years marine controlled-source electromagnetic (MCSEM) surveys have become widely used for offshore petroleum exploration. The main target of this survey is the sea-bottom petroleum reservoir, which is usually characterized by a low electrical conductivity anomaly within relatively conductive sea-bottom sediments. There is growing interest in the interpretation of MCSEM data based on 3D geoelectrical models. The conventional approach based on standard 3D forward modeling and inversion meets significant difficulties because of

[a] Department of Geology and Geophysics, University of Utah, USA
[b] Center for High Performance Computing, University of Utah, USA
[c] Geological Survey of Japan, Japan

E-mail address: mzhdanov@mines.utah.edu (M.S. Zhdanov).

Handbook of Geophysical Exploration: Seismic Exploration, Volume 40
ISSN 0950-1401, DOI: 10.1016/S0950-1401(10)04023-1

© 2010 Elsevier Ltd.
All rights reserved.

the enormous amount of computations required in the case of the multitransmitter and multireceiver data acquisition systems typical for marine CSEM surveys.

There is an alternative approach to the solution of this problem, which is based on the ideas of electromagnetic holography and/or migration (Zhdanov, 1981; Zhdanov and Frenkel, 1983a,b; Zhdanov, 1988; Zhdanov and Keller, 1994; Zhdanov et al., 1996; Zhdanov and Traynin, 1997; Zhdanov, 1999, 2001, 2002; Tompkins, 2004; Mittet et al., 2005; Wan and Zhdanov, 2005a,b; Zhdanov et al., 2006).

The physical principles of EM holography parallel those underlying optical holography and seismic migration. The recorded amplitudes and phases of an EM field scattered by an object form a broadband EM hologram. As in optical and radiowave holography, we can reconstruct the volume image of the object by "illuminating" the broadband EM hologram by a reference signal. While in the optical case this can be performed optically, yielding a visible image, in the case of a broadband EM field the reconstruction is done numerically, using computer transformation. In fact EM holography/migration, similar to seismic migration, is based on a special form of downward continuation of the observed field, which can be computed as a solution of the boundary value problem for the adjoint Maxwell's equations.

In the current paper we consider an application of this approach to the interpretation of a typical sea-bed logging (SBL) survey which consists of a set of sea-bottom receivers and a moving electrical bipole transmitter. The receivers record the magnitude and the phase of the frequency domain (FD) electromagnetic field generated by the moving transmitter and scattered back by sea-bottom geoelectrical structures. The combined electromagnetic signal in the receivers forms a broad-band EM hologram of the sea-bottom geological target (e.g., a petroleum reservoir). In order to reconstruct the geoelectrical image of the target, we replace a set of receivers with a set of auxiliary transmitters located in the positions of the receivers. The strength and the phase of the signal transmitted by these auxiliary transmitters are determined according to the parameters of the observed field in the receivers. These transmitters generate an EM field, which is called a backscattering or migration field. The vector cross-power spectrum of the background field (the field generated by the original transmitter in a medium without a target) and the backscattering field produces a numerical reconstruction of a volume image of the conductivity distribution (Zhdanov, 2001).

We should note, however, that the frequency of the EM signal used in a marine EM is very low, about 1 Hz. In this low frequency range, the EM field propagates in sea-bottom formations according to the diffusion equation (Zhdanov and Keller, 1994), which results in a relatively low resolution of the geoelectrical image obtained by the numerical algorithm described above. In order to improve the resolution of the EM holographic

the case of the
systems typical for

problem, which
and/or migration
1988; Zhdanov
Traynin, 1997;
al., 2005; Wan and

those underlying
amplitudes and
a broadband EM
can reconstruct the
EM hologram
can be performed
broadband EM field
transformation. In
is based on a
field, which can
problem for the adjoint

approach to the
which consists of a
transmitter. The
frequency domain (FD)
transmitter and scattered
electromagnetic
of the sea-bottom
in order to reconstruct
set of receivers with
positions of the receivers.
by these auxiliary
parameters of the observed
EM field, which is
cross-power spectrum
original transmitter in a
produces a numerical
distribution (Zhdanov,

the EM signal used in
frequency range, the
according to the diffusion
results in a relatively low
numerical algorithm
the EM holographic

imaging, we should apply the migration iteratively. The development of the corresponding method of iterative migration with application to MCSEM data constitutes the main subject of the present paper.

2. Marine Controlled-Source Electromagnetic (MCSEM) Method

The MCSEM method for hydrocarbon exploration has a long history that stretches back to the beginning of the 20th century (Berdichevsky et al., 1989; Srnka et al., 2006). One can look back to the beginning of marine CSEM research more than 80 years ago with direct current (DC) surveys off the Cornish coast of England. Significant progress, however, was only made in the 1960s and 1970s through efforts by university and government groups, especially for pure geophysical, earth science research, based mainly on the natural marine magnetotelluric (MMT) method (e.g., Novysh and Fonarev, 1966; Trophimov and Fonarev, 1972). There have been several EM methods for mapping and imaging sub-sea-bottom geoelectrical structures (e.g., Sinha et al., 1990; Chave et al., 1991), especially for application to the study of the oceanic lithosphere and actively spreading mid-ocean ridges (Young and Cox, 1981; Evans et al., 1994; Constable and Cox, 1996; MacGregor and Sinha, 2000; MacGregor et al., 2001). Marine geoelectrical investigations have been intensively developed in the former Soviet Union. A review of this research can be found in Berdichevsky et al. (1989).

The turning point for the marine CSEM method came almost 25 years ago. According to Srnka et al. (2006), at the beginning of the 1980s major western oil companies began investigating marine CSEM theory and computer modeling. The companies found results that looked promising for deep-water applications (i.e., the deeper the water, the better), and field tests were proposed over the known reservoirs. The conclusion of the companies at that time was, however, that the time for marine CSEM in the petroleum industry had not yet arrived; this was mainly due to the lack of suitable acquisition equipment, inadequate computational capability, a rapidly growing emphasis on the new, powerful 3D marine seismic technology, and limited deep-water business opportunities. As a result, marine CSEM research was deferred. For about the last 20 years the 3D seismic survey has been a de facto standard and priority choice for offshore hydrocarbon exploration with the cooperation of gravity/magnetic and well logging.

We should note, however, that Russian geophysicists had used marine EM for HC exploration since the early 1970s. In the latter half of the 1990s, western oil and gas companies found that, in some potential hydrocarbon reservoir areas, the seismic method had failed to detect the hydrocarbons, or did not have enough resolution because of a complicated

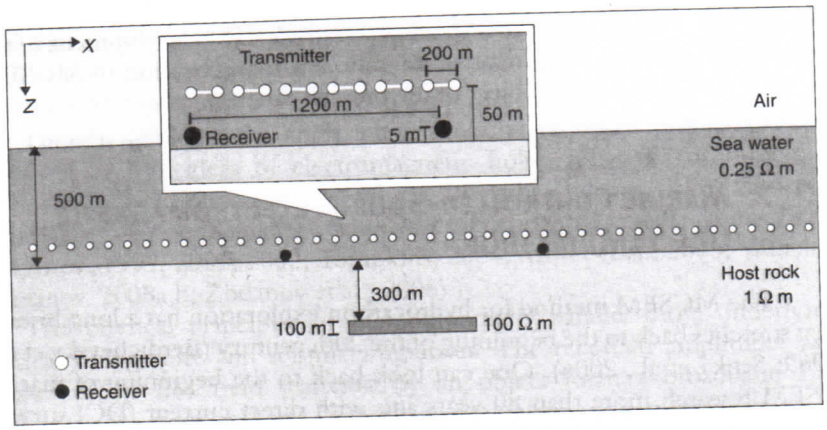

Figure 1 Sketch of the SBL survey and model design.

subsurface structure. Therefore, several research projects were initiated to find appropriate exploration techniques in such areas, including re-examination of marine EM methods around the world—not only by the academic community, but also by several major western petroleum companies. During the past two decades, great advances in both equipment and computational resources have created a favorable wind for EM methods, especially the MCSEM method for petroleum exploration.

3. Frequency Domain Electromagnetic (FDEM) Migration of MCSEM Data

Let us consider a typical MCSEM survey consisting of a set of electric field receivers located at the sea bottom and an electric bipole transmitter moving at some elevation above the sea bottom, as shown in Figure 1. We assume that the electrical conductivity in the model can be represented as the sum of the background conductivity $\sigma = \sigma_b$ and an anomalous conductivity $\Delta\sigma$ distributed within some local inhomogeneity D associated with the location of the petroleum reservoir.

The background conductivity is formed by a horizontally layered model consisting of nonconductive air, a conductive seawater layer, and a horizontally homogeneous (layered) section of a sea-bottom formation. The receivers are located at points with radius-vector r_j $(j = 1, 2, 3, \ldots, J)$ in some Cartesian coordinate system. Every receiver R_j records electric and magnetic field components of the field generated by an electric bipole transmitter moving above the receivers. We denote this field as $\mathbf{E}_i(r_j)$, $\mathbf{H}_i(r_j)$, where i is the index of the corresponding transmitter, T_i, located at the point $\mathbf{r}_i$ $(i = 1, 2, 3, \ldots, I)$.

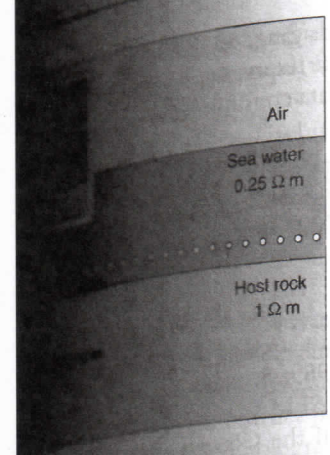

were initiated
areas, including re-
world—not only by
western petroleum
in both equipment
for EM methods,

AGNETIC (FDEM)

of a set of electric
bipole transmitter
shown in Figure 1. We
be represented as the
anomalous conductivity
associated with the

horizontally layered
seawater layer, and a
bottom formation. The
$j = 1, 2, 3, \ldots, J$)
R_j records electric
an electric bipole
this field as $\mathbf{E}_i(r_j)$,
transmitter, T_i, located

Let us consider the data observed by one receiver, R_j. According to the reciprocity principle, the electric field component excited at $\mathbf{r}_j$ in the direction of $\mathbf{b}$ by an electric current element $\mathbf{a}$ at $\mathbf{r}_i$ is identical to the electric field component excited at $\mathbf{r}_i$ in the direction of $\mathbf{a}$ by an electric current element $\mathbf{b}$ at $\mathbf{r}_j$ (Zhdanov, 2002, p. 226):

$$\mathbf{E}_i(\mathbf{r}_j) \cdot \mathbf{b} = \mathbf{E}_j^E(\mathbf{r}_i) \cdot \mathbf{a}. \tag{1}$$

Similarly, the magnetic field component excited at $\mathbf{r}_j$ in the direction of $\mathbf{b}$ by an electric current element $\mathbf{a}$ at $\mathbf{r}_i$ is equal to the electric field component (multiplied by the minus sign) excited at $\mathbf{r}_i$ in the direction of $\mathbf{a}$ by a magnetic current element $\mathbf{b}$ at $\mathbf{r}_j$:

$$\mathbf{H}_i(\mathbf{r}_j) \cdot \mathbf{b} = -\mathbf{E}_j^H(\mathbf{r}_i) \cdot \mathbf{a}. \tag{2}$$

Therefore, one can substitute a reciprocal survey configuration for the original survey, assuming that we have electric, T_j^E, and magnetic, T_j^H, dipole transmitters located in the position of the receiver, R_j, and a set of receivers measuring the reciprocal electric fields, $\mathbf{E}_j^E(\mathbf{r}_i)$ and $\mathbf{E}_j^H(\mathbf{r}_i)$ in the positions of the original transmitters, T_i.

We can now calculate the backscattering (or migration) field for the data collected by one fixed sea-bottom receiver, R_j. Consider, for example, the reciprocal electric fields $\mathbf{E}_j^E(\mathbf{r}_i)$. This field can be represented as the sum of the background and anomalous parts:

$$\mathbf{E}_j^E(\mathbf{r}_i) = \mathbf{E}_j^b(\mathbf{r}_i) + \mathbf{E}_j^{E_a}(\mathbf{r}_i), \tag{3}$$

where the background electric field, $\mathbf{E}_j^b(\mathbf{r}_i)$ is generated by the electric dipole transmitter T_j^E in a model with a given background conductivity σ_b. The residual electric field, $\mathbf{R}_{E_j}(\mathbf{r}_i)$ is equal to the difference between the background and "observed" reciprocal field:

$$\mathbf{R}_{E_j}(\mathbf{r}_i) = \mathbf{E}_j^b(\mathbf{r}_i) - \mathbf{E}_j^E(\mathbf{r}_i) = -\mathbf{E}_j^{E_a}(\mathbf{r}_i). \tag{4}$$

According to the definition (Zhdanov, 2002), the backscattering (migrated) residual field is a field generated in the background medium by a combination of all electric dipole transmitters located at points $\mathbf{r}_i$ with the current moments determined by the complex conjugate residual field

$\mathbf{R}^*_{E_j}(\mathbf{r}_i)$ according to the following formula:

$$\mathbf{E}^m_j(\mathbf{r}) = \mathbf{E}^m_j(\mathbf{r}; \mathbf{R}^*_{E_j}) = \sum_{i=1}^{I} \mathbf{G}_E(\mathbf{r}|\mathbf{r}_i)\mathbf{R}^*_{E_j}(\mathbf{r}_i), \tag{5}$$

where the lower subscript j shows that we migrate the field observed by the receiver R_j, and $\mathbf{G}_E$ is the electric Green's tensor for the layered (background) conductivity model σ_b. Therefore, the migration field can be computed as a superposition of 1D weighted (by the corresponding receiver residual) responses generated by electric dipoles with the unit moments located at every transmitter position in the model with the background conductivity σ_b. This 1D electric dipole modeling is a very fast process, which results in the fast migration algorithm.

Formula (5) allows us to reconstruct the migration field everywhere in the medium under investigation. It can be shown that this transformation is stable with respect to the noise in the observed data. At the same time the spatial distribution of the migration field is closely related to the conductivity distribution in the medium. However, one needs to apply the corresponding imaging conditions to enhance the conductivity image produced by the EM migration. We will discuss this problem in the following sections of the paper.

In the general case of multiple receivers, the migration field is generated in the background medium by all electric dipole transmitters located above all receivers, R_j, having the current moments determined by the complex conjugate residual field $\mathbf{R}^*_{E_j}(\mathbf{r}_i)$:

$$\mathbf{E}^m(\mathbf{r}) = \sum_{j=1}^{J}\sum_{i=1}^{I} \mathbf{G}_E(\mathbf{r}|\mathbf{r}_i)\mathbf{R}^*_{E_j}(\mathbf{r}_i). \tag{6}$$

According to formula (5), we have:

$$\mathbf{E}^m(\mathbf{r}) = \sum_{j=1}^{J} \mathbf{E}^m_j(\mathbf{r}). \tag{7}$$

Therefore, the total migration field for all receivers can be obtained by summation of the corresponding migration field computed for every individual receiver.

A remarkable fact is that the migration of both electric and magnetic field data is actually reduced to the same forward problem for the electric field generated by the electric dipole transmitters. The only difference is that, in the case of the electric field receivers, we use the electric observed data

to determine the electric current moment in the reciprocal transmitters. In the case of the magnetic receivers, the observed magnetic data are used to determine electric current moments of the receivers.

4. Electromagnetic Imaging Using Joint Migration of Electric and Magnetic Fields

The principles of EM holography/migration imaging are very similar to those of optical holography (Zhdanov, 2001). They can be summarized as follows.

(1) We "illuminate" the background media by a reciprocal electric dipole (in the case of electric observations) located in the actual receivers' positions to generate the "electric mode" background EM field $\{\tilde{\mathbf{E}}^{bE}, \tilde{\mathbf{H}}^{bE}\}$. Alternatively, we "illuminate" the background media by a reciprocal magnetic dipole (in the case of the magnetic field observations) located in the actual receivers' positions to generate the "magnetic mode" background EM field $\{\tilde{\mathbf{E}}^{bE}, \tilde{\mathbf{H}}^{bE}\}$.

(2) We "illuminate" the background media by artificial transmitters located in the positions of the true transmitters and represented by equivalent (fictitious) electric current dipoles. In the case of electric observations, the current moments are determined by the complex conjugate anomalous electric field observed in the true receiver for the given transmitter position. The electromagnetic field produced by this system of artificial electric dipoles generates the "electric mode" migration (backscattering) anomalous field $\{\tilde{\mathbf{E}}^{mE}, \tilde{\mathbf{H}}^{mE}\}$. In the case of magnetic observations, the current moments are determined by the complex conjugate anomalous electric field multiplied by the factor $(-i\omega\mu)$. The electromagnetic field produced by this system of artificial transmitters generates the "magnetic mode" migration (backscattering) anomalous field $\{\tilde{\mathbf{E}}^{mE}, \tilde{\mathbf{H}}^{mE}\}$.

(3) In the case of electric field observations, the geoelectrical image of the sea-bottom inhomogeneities, $\mathbf{I}_0^E$, is formed by summation of the cross-power spectrum of the "electric mode" background and migration fields:

$$\mathbf{I}_0^E = \mathrm{Re}\,\Sigma_{\omega_n}\left(\tilde{\mathbf{E}}^{bE} \cdot \tilde{\mathbf{E}}^{mE}\right), \tag{8}$$

where summation is done over all frequencies ω_n of the recorded fields.

(4) In the case of magnetic field observations, the geoelectrical image of the sea-bottom inhomogeneities, $\mathbf{I}_0^H$ is formed by calculating the cross-power spectrum of the "magnetic mode" background and migration

fields:

$$\mathbf{I}_0^H = \mathrm{Re}\,\Sigma_{\omega n}\left(\tilde{\mathbf{E}}^{bH}\cdot\tilde{\mathbf{E}}^{mH}\right). \tag{9}$$

(5) In the case of joint migration of the electric and magnetic observed data, the geoelectrical image of the sea-bottom inhomogeneities, $\mathbf{I}_0^{EH}$, is formed by summation of the "electric mode" and "magnetic mode" images:

$$\mathbf{I}_0^{EH} = \mathrm{Re}\,\Sigma_{\omega n}\left[\left(\tilde{\mathbf{E}}^{bE}\cdot\tilde{\mathbf{E}}^{mE}\right)+\left(\tilde{\mathbf{E}}^{bH}\cdot\tilde{\mathbf{E}}^{mH}\right)\right]. \tag{10}$$

Note that, in the case of multireceiver observations, the final image is produced by summation of all migration images generated for each receiver.

The images generated by formulas (8) to (10) are usually slightly distorted due to the different sensitivities of the observed data to the geoelectrical anomalies located at different depths and at different horizontal positions. To account for different sensitivities of the data to the conductivity distribution, we use an additional weighting function, W_m:

$$\sigma \approx -k(\mathbf{W}_m^*\mathbf{W})^{-1}\mathbf{I}_0, \tag{11}$$

where stands for any of the migration images introduced above, and k is some scaling coefficient.

The model parameter weighting matrix W_m is computed using the integrated sensitivity $\mathbf{S}$ as follows:

$$\mathbf{W}_m = \mathbf{S}^{\frac{1}{2}}, \tag{12}$$

where the integrated sensitivity is determined using the following formula (Zhdanov, 2002, p. 80):

$$\mathbf{S} = \mathrm{diag}(\mathbf{F}^*\mathbf{F})^{\frac{1}{2}}. \tag{13}$$

In the last formula, $\mathbf{F}$ stands for the Fréchet derivative matrix of the corresponding EM forward modeling operator. By weighting the migration image $\mathbf{I}_0^{EH}$ with the integrated sensitivity, we assure that the observed data are equally sensitive to the conductivity variations within every part of the domain of investigation. As a result, we generate the electrical conductivity image which correctly reflects the volume distribution of the anomalous conductivity.

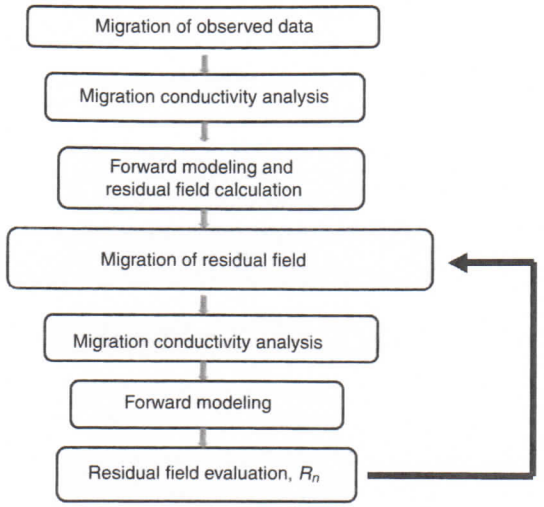

Figure 2 A scheme of the computational flow for iterative migration.

5. Regularized Iterative Migration

We have demonstrated above that migration imaging can be treated as the first iteration in the solution of the electromagnetic inverse problem. Obviously, we can obtain better imaging results if we repeat the iterations. Following Zhdanov (2002), we can describe the method of iterative migration as follows. On every iteration we calculate the theoretical electromagnetic response $\tilde{\mathbf{E}}_n$ for the given geoelectrical model σ_n, obtained in the previous step, we calculate the residual field between this response and the observed field, $\tilde{\mathbf{R}}_E^n$ and then we migrate the residual field. The geoelectrical image is computed, according to Eq. (8), as a sum over the frequencies of the dot product of the migrated residual field and the theoretical response $\tilde{\mathbf{E}}^n$. This image is corrected by the integrated sensitivity $\mathbf{S}$ to calculate the new geoelectrical model σ_n on the basis of expression (11). Iterative migration is terminated when the residual field becomes smaller than the required accuracy level of the data fitting. Figure 2 shows a scheme of the computational flow for iterative migration.

In fact, iterative migration results in rigorous inversion. It was demonstrated in Portniaguine and Zhdanov (1999) and Zhdanov (2002) that images with sharp boundaries can be recovered by regularized inversion algorithms based on a special family of stabilizing functionals. Particularly, the minimum support (MS) functional was found to be useful in the solution of this problem. It selects the inverse model within the class of models with

a minimum volume of a domain with anomalous parameter distribution. This class of models describes the compact objects which are typical targets, for example, in mineral and hydrocarbon exploration. A similar approach can be applied in the case of the iterative migration transformation. We call this technique focusing iterative migration. Numerical implementation of focusing migration is similar to focusing inversion (Zhdanov, 2002). Particularly, images with sharp boundaries can be recovered using the minimum support (MS) or minimum gradient support (MGS) stabilizing functionals. This technique is implemented in our algorithm of focusing migration of electric and magnetic field data.

Another advantage of iterative migration is based on the fact that it allows us to include an a priori model of the target in the iterative process in a similar way as in the case of conventional inversion. The details of this technique can be found in (Zhdanov, 2002).

Note that every iteration of the migration algorithm requires two forward modeling computations: one to compute the migration field, and another one to compute the predicted data in the receivers. In this work, we use recently developed migration code that is parallelized over the Z dimension of the migration domain. For calculation of the migration and predicted fields we use an integral equation (IE) based on a parallel computer program. This enables us to considerably reduce the computation time and also model larger problems by increasing the migration domain size and the number of the cells used for the migration domain discretization.

6. Migration of Synthetic MCSEM Data

We have analyzed the principles of the iterative EM migration outlined above using as an example synthetic MCSEM data, computed for the models shown below.

6.1. Model 1

In the first set of numerical experiments, we assume that a synthetic MCSEM survey is conducted in relatively shallow water with a sea depth of 300 m. The survey consists of eleven sea-bottom receivers and an electric dipole transmitter moving along a line passing directly above the receivers at an elevation 50 m above the seafloor. The transmitter generates a frequency domain EM field every 200 m along the towing line, which is extended from -3000 m to 3000 m. Eleven seafloor electric receivers are located 5 m above the sea bottom along the x coordinates from $x = -2500$ m to $x = 2500$ m with a 500 m spacing. The background layered geoelectrical model consists of a seawater layer with a thickness of 300 m, a resistivity of 0.25 Ohm m, and homogeneous sea-bottom sediments with a resistivity of 1 Ohm m. There is

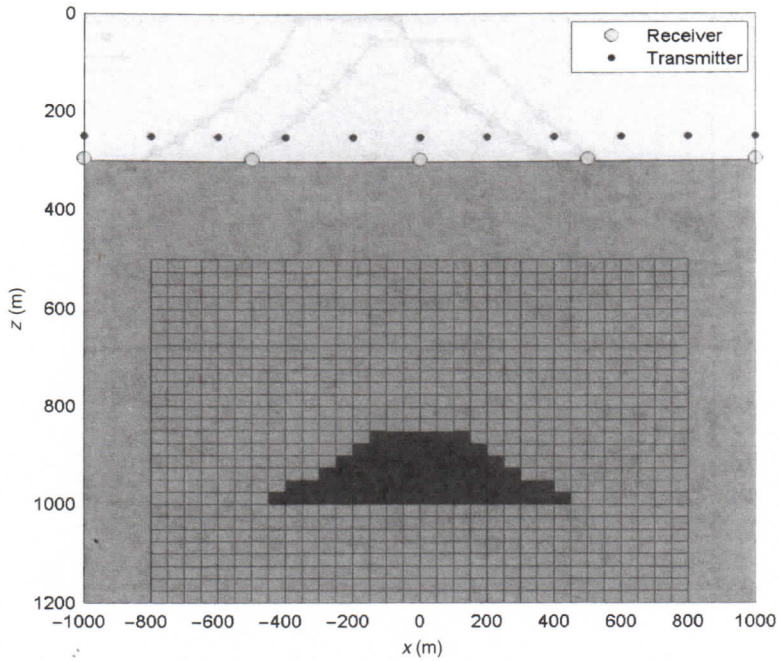

Figure 3 A vertical section of the true resistivity model along the survey line. The reservoir resistivity (blue) is 100 Ohm m, the background resistivity (red) is 1 Ohm m.

an anticlinal oil reservoir located in the seafloor sediments at a depth between 850 m and 1000 m below the sea level with a resistivity of 100 Ohm m and a maximum horizontal diameter of 900 m. A vertical section of the true resistivity model along the survey line is shown in Figure 3. The migration domain is discretized with a cell size of $25 \times 25 \times 25$ m^3 resulting in 28,672 cells.

The transmitter generates an EM field at frequencies of 0.25 and 0.75 Hz. The receivers measure the in-line component of the electric fields, E_x, and the cross-line component of the magnetic fields, H_y, simultaneously. The synthetic MCSEM data for this model were calculated using the parallel integral equation forward modeling code PIE3D developed by Yoshioka and Zhdanov (2005).

The observed data for this model can be represented as the plots of the total electric field E_x and magnetic field H_y recorded in the receivers, the plots of the same fields normalized by the absolute values of the background electric and magnetic fields respectively, and the plots of the phase difference between the observed and background electric fields (Figures 4 through 7). We show magnitude versus offset (MVO) and phase versus offset (PVO) plots of the total and normalized fields in these figures. Note that we have

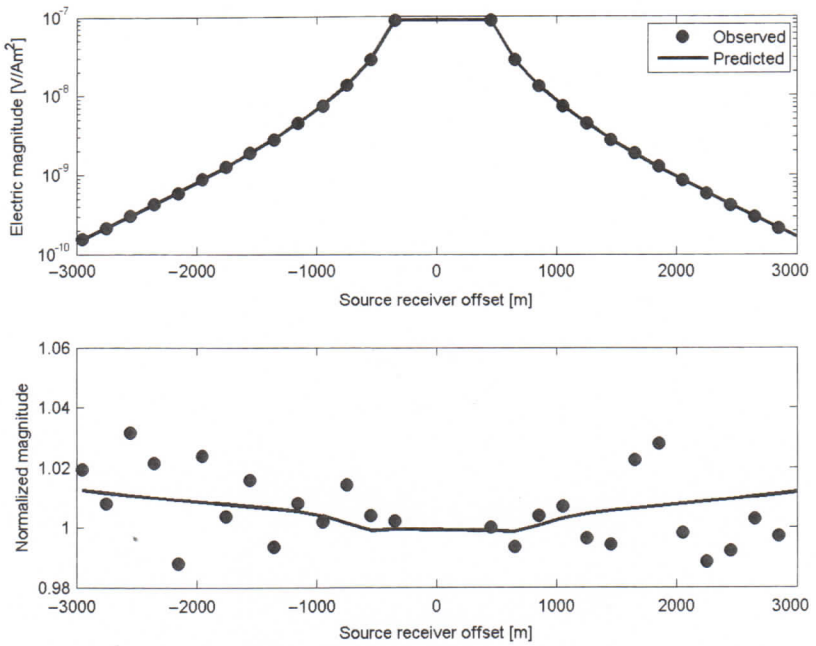

Figure 4 The top panel shows magnitude versus offset (MVO) plots of the total electric field, while the bottom panel presents the MVO plot of the same field normalized by the absolute values of the background electric fields. The observed data contaminated by noise are shown by the dots. The solid line corresponds to the data predicted for the migration resistivity model.

contaminated the synthetic observed data with random Gaussian noise. The noise level increases linearly from 1% at zero offset up to 7% at 10,000 m offset to simulate the typical noise behavior in the field MCSEM data.

We consider a 3D migration of the electric and magnetic field data for Model 1. We can realize a full 3D migration for the data observed by a few receivers located along a profile, because we generate a 3D migration field by a set of reciprocal transmitters. The migration field generated by these transmitters propagates within the medium in all directions, creating a 3D image of the target.

We perform two iterative migration calculations. The first calculation uses no a priori model. We run 35 iterations of the migration. The location and shape of the reservoir are resolved fairly well (Figure 8). The holographic image is slightly too deep and the smaller upper part is not visible.

In the second calculation, we have used an anticlinal a priori model with resistivity 3 Ohm m that encloses the true reservoir. We again ran 35 iterations. However, the a priori model was used only during the 30 initial iterations. The reservoir location is now resolved much clearer (Figure 9). Figures 4 through 7 show the predicted data computed for the migration

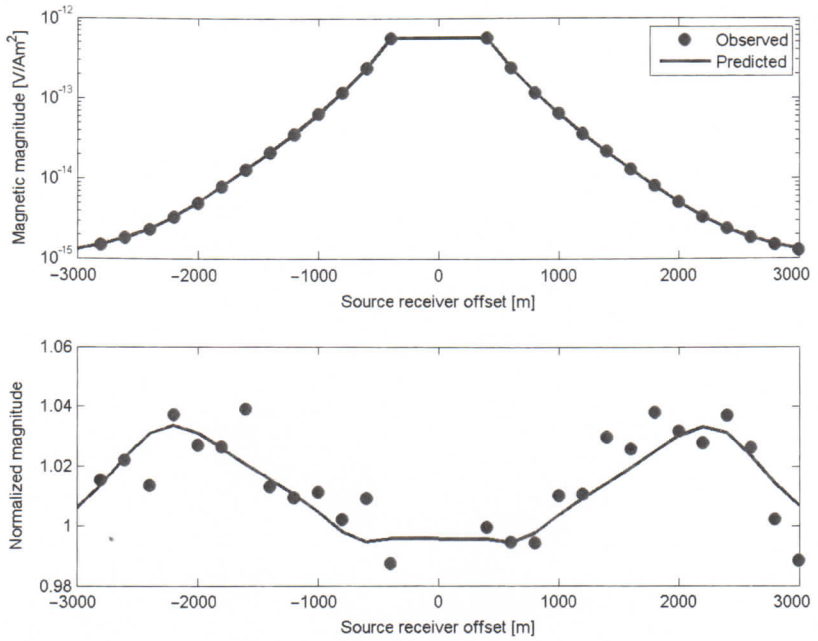

Figure 5 The top panel shows magnitude versus offset (MVO) plots of the total magnetic field, while the bottom panel presents the MVO plot of the same field normalized by the absolute values of the background magnetic fields. The observed data contaminated by noise are shown by the dots. The solid line corresponds to the data predicted for the migration resistivity model.

model shown in Figure 9. The predicted data show a good fit to the noisy observed data.

6.2. Model 2

In the second test of the numerical experiments, we consider a geoelectrical model of the sea-bottom formation shown in Figure 10. The MCSEM survey consists of two parallel transmitter-receiver profiles in the x direction. Each line consists of five sea-bottom receivers and an electric dipole transmitter moving along a line passing directly above the receivers at an elevation 50 m above the seafloor. In order to reduce the calculation cost, we assume that the transmitter generates a frequency domain EM field every 500 m along the towing line, which is extended from −4000 m to 4000 m. A total of ten seafloor electric receivers are located 5 m above the sea bottom along the x coordinates from $x = -2000$ to $x = 2000$ m with a 1000 m spacing at $y = -500$ m and $y = +500$ m. The background layered geoelectrical model consists of a seawater layer with a thickness of 300 m, a resistivity of 0.25 Ohm m, and homogeneous sea-bottom sediments with a

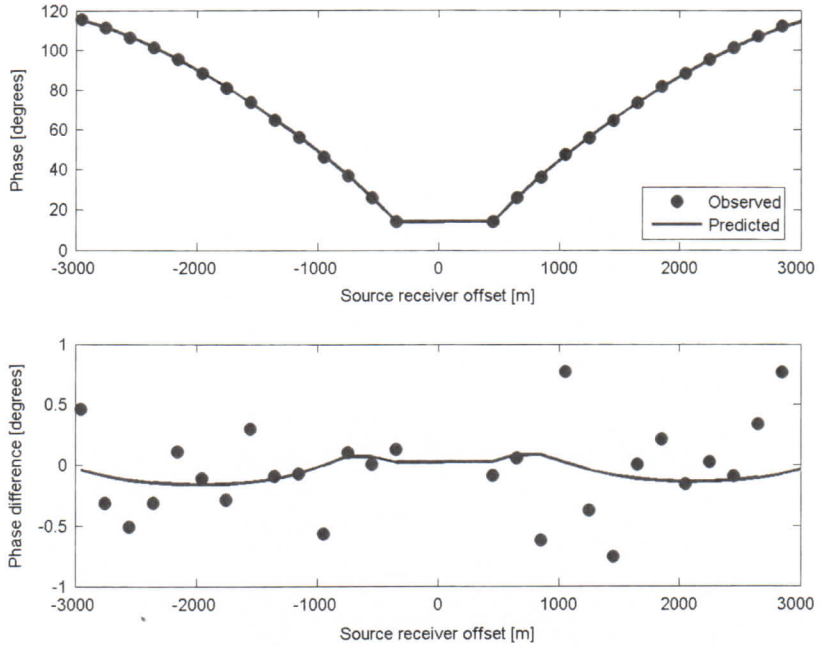

Figure 6 The top panel shows phase versus offset (PVO) plots of the total electric field, while the bottom panel presents the PVO plot of the phase difference between the observed and background electric fields. The observed data contaminated by the noise are shown by the dots. The solid line corresponds to the data predicted for the migration resistivity model.

resistivity of 1 Ohm m. There is an L-shaped reservoir located in the seafloor sediments at a depth between 800 m and 1000 m below sea level with a resistivity of 100 Ohm m, and a horizontal size of 2000 m by 2000 m. A 3D sketch of the true resistivity model and transmitter-receiver locations is shown in Figure 10. The size of the cells in the migration domain is $100 \times 100 \times 25$ m^3 resulting in 44,800 cells.

The transmitter generates an EM field at frequencies of 0.125, 0.25 and 0.75 Hz. The receivers measure the in-line component of the electric fields, E_x, and the cross-line component of the magnetic fields, H_y, simultaneously.

We present in Figures 11 and 12 the observed electric data for this model, as an example. We show magnitude versus offset (MVO) and phase versus offset (PVO) plots of the total and normalized fields in these figures. Note that we have contaminated the synthetic observed data with random Gaussian noise. The noise level increases linearly from 1% at zero offset up to 7% at 10,000 m offset to simulate the typical noise behavior in field MCSEM data.

We apply the joint 3D migration to the electric and magnetic data with an L-shaped a priori model that encloses the true reservoir and has a

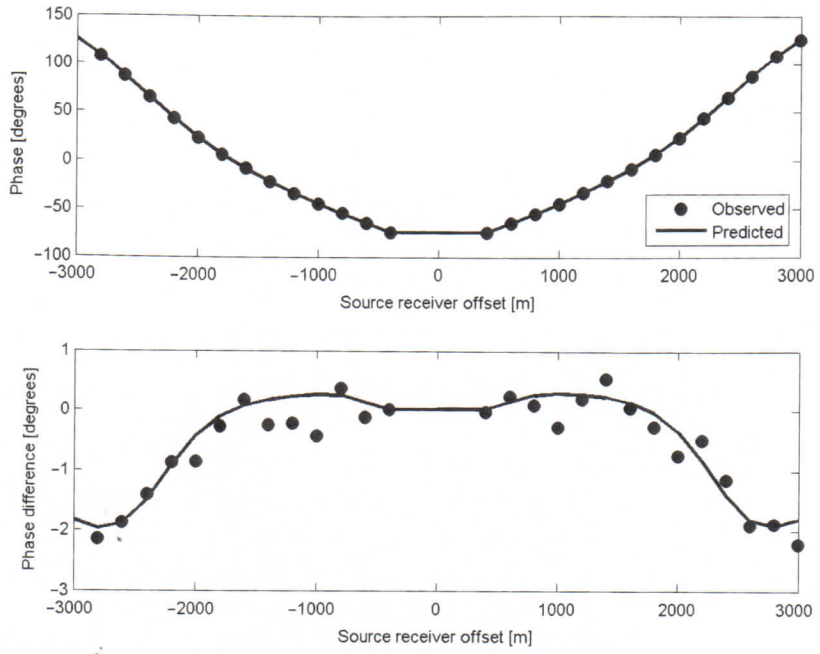

Figure 7 The top panel shows phase versus offset (PVO) plots of the total magnetic field, while the bottom panel presents the PVO plot of the phase difference between the observed and background magnetic fields. The observed data contaminated by the noise are shown by the red dots. The blue solid line corresponds to the data predicted for the migration resistivity model.

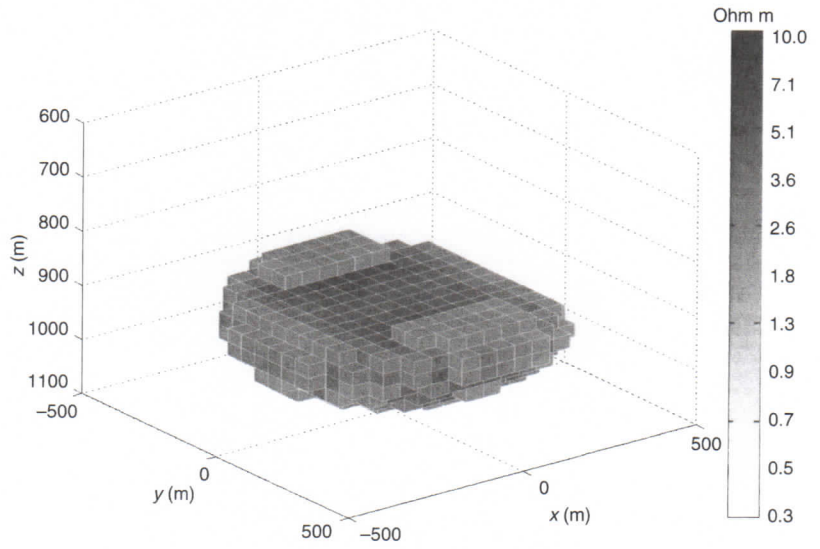

Figure 8 Final 3D holographic image of Model 1 without using an a priori model.

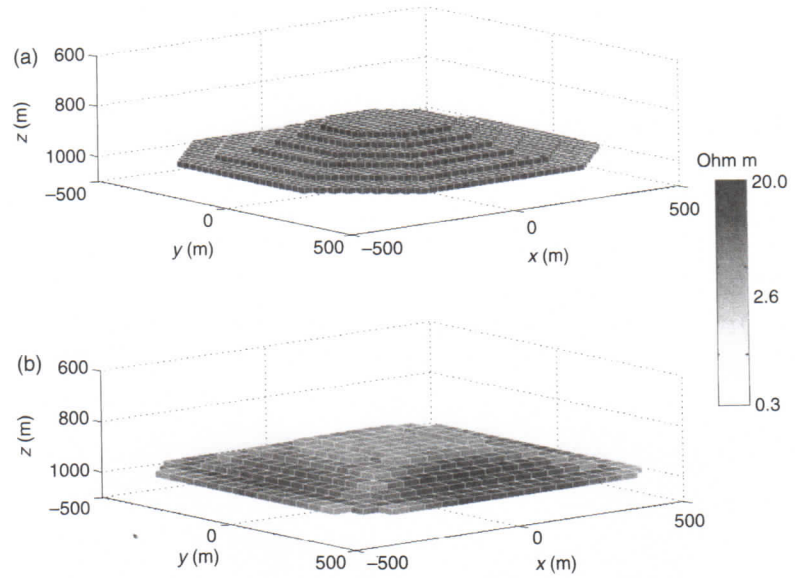

Figure 9 The figure shows (a) the true model and (b) the final 3D holographic image obtained by joint iterative migration of the EM data for Model 1.

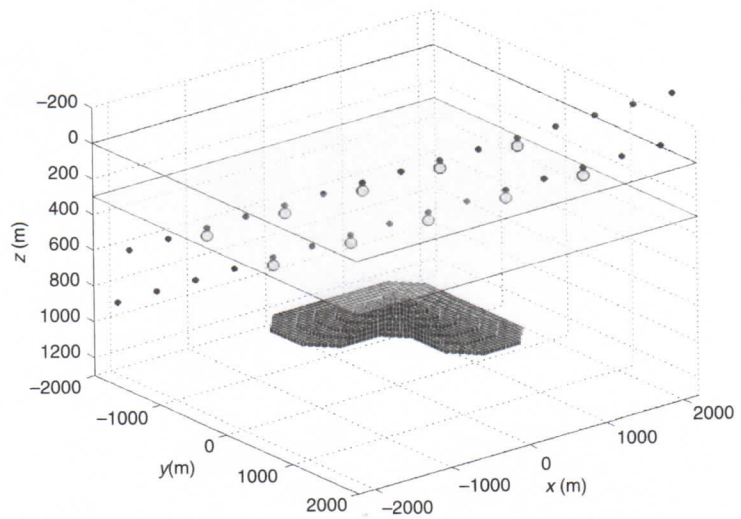

Figure 10 A 3D sketch of Model 2. The blue dots show the transmitter towing profiles and the green dots show the location of a sea-bottom receiver. The host rock has a resistivity of 1 Ohm m, while the resistivity of the L-shaped reservoir is 100 Ohm m.

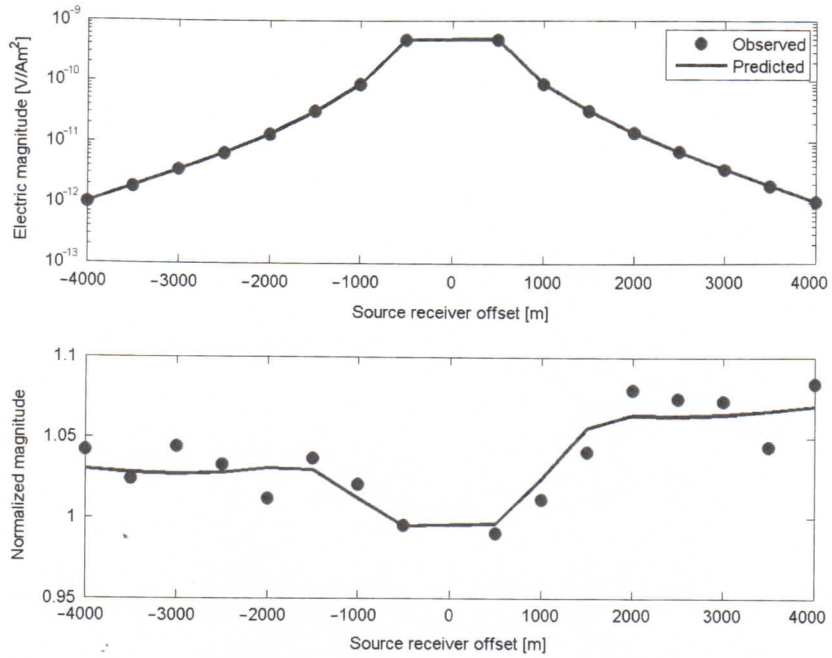

Figure 11 The top panel shows magnitude versus offset (MVO) plots of the total electric field, while the bottom panel presents an MVO plot of the same field normalized by the absolute values of the background magnetic field. The observed data contaminated by noise are shown by the dots. The solid line corresponds to the data predicted for the migration resistivity model.

resistivity of 3 Ohm m. We ran 35 iterations of focusing migration. The a priori model was applied only for the 30 initial iterations. The normalized residual reaches 8% at iteration #35. The corresponding holographic image is shown in Figure 13 as an X-Y plan view at a depth of $z = 962.5$ m and in Figure 14 as a 3D rendering of the true body and migration result. The shape of the recovered reservoir is close to the a priori model but we notice at the corners of the reservoir smaller resistivity values, which are rounded in the true model. Also, the smaller top of the reservoir is not recovered as well as the thicker bottom. We have also plotted in Figures 11 and 12 the predicted data computed for the migration model shown in Figure 14.

7. Inversion of Troll Gas Province MCSEM Data

We have applied the 3D EM migration techniques, including both fast migration imaging and iterative migration, to the interpretation of marine

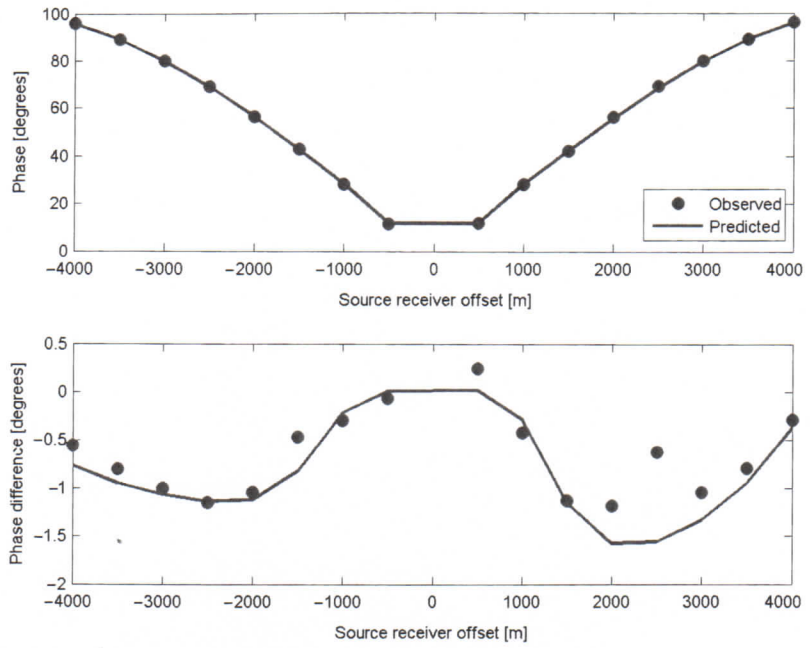

Figure 12 The top panel shows phase versus offset (PVO) plots of the total electric field, while the bottom panel presents a PVO plot of the phase difference between the observed and background magnetic fields. The observed data contaminated by noise are shown by the dots. The solid line corresponds to the data predicted for the migration resistivity model.

EM data collected by EMGS and Statoil at the Troll West Gas Province (TWGP), offshore Norway (Johansen et al., 2005).

The Troll province is located in the northeastern part of the North Sea (Figure 15). This reservoir area is the largest gas discovery on the Norwegian Continental Shelf. The Troll province is separated into three subregions such as Troll East, Troll West Gas Province (TWGP) and Troll West Oil Province (TWOP), as shown in Figure 16. The Seabed Logging (SBL - a trademark of the MCSEM survey) was conducted over the smaller section of TWGP shown in Figure 17. The hydrocarbon reservoir is formed by Jurassic sandstones with a gas layer of up to 160 m. The sandstone saturated with hydrocarbon sands is characterized by a high average resistivity in the range of 200-500 Ohm m. This highly resistive layer is located at a depth of 1400 m below sea level (1100 m below the seafloor). The host sand sediments are filled with saline water and have relatively low resistivity in the range of 0.5-2 Ohm m. Geoelectrical structures such as this highly resistive hydrocarbon target within conductive background sediments makes TWGP very well suited for the MCSEM field test.

A marine CSEM survey was conducted using 24 receivers, deployed at the sea bottom along a line crossing the Western Gas Province. The

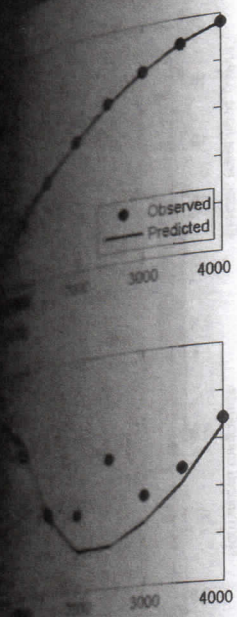

...total electric field, ...between the observed ...are shown by the ...resistivity model.

...West Gas Province

...part of the North Sea ...very on the Norwegian ...three subregions ...and Troll West Oil ...Logging (SBL - a ...smaller section of ...formed by Jurassic ...saturated with ...resistivity in the range ...a depth of 1400 m ...and sediments are ...in the range of 0.5- ...hydrocarbon ...TWGP very well

...receivers, deployed ...Gas Province. The

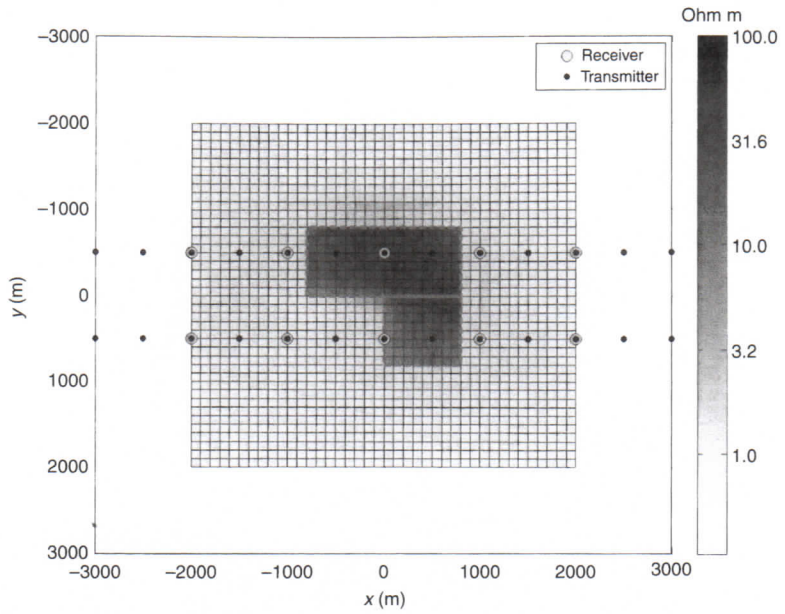

Figure 13 2D X-Y plan view images of the final joint iterative migration result for Model 2 obtained by 3D migration of the EM fields.

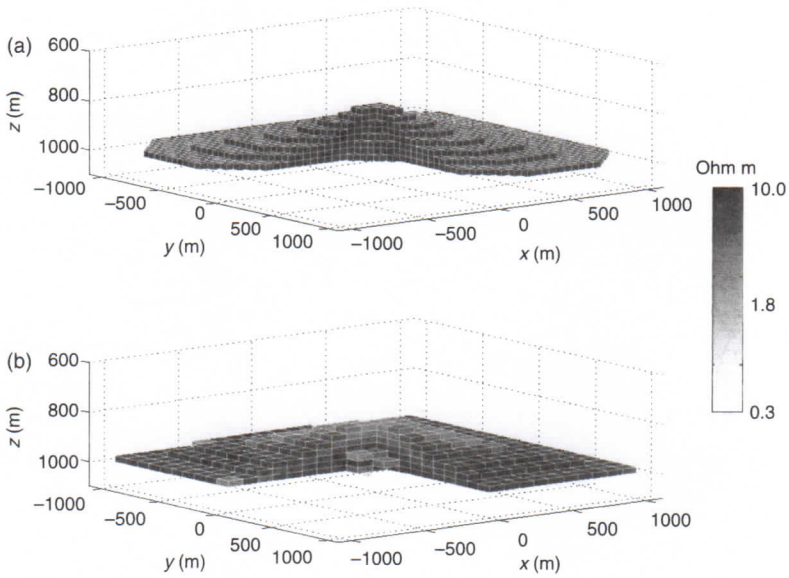

Figure 14 3D images of (a) the true model and (b) the final joint iterative migration result for Model 2 obtained by 3D migration of the EM fields.

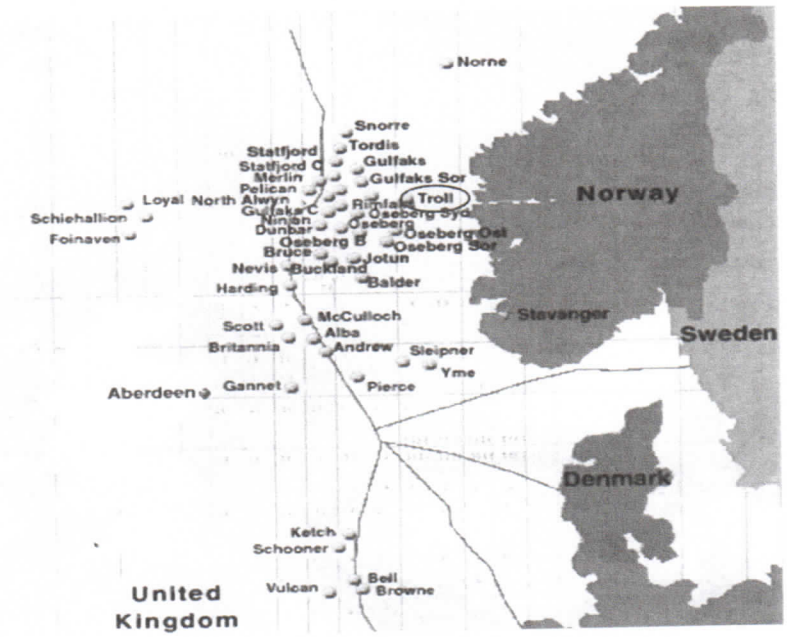

Figure 15 A map of the Troll West Gas Province (TWGP) location.

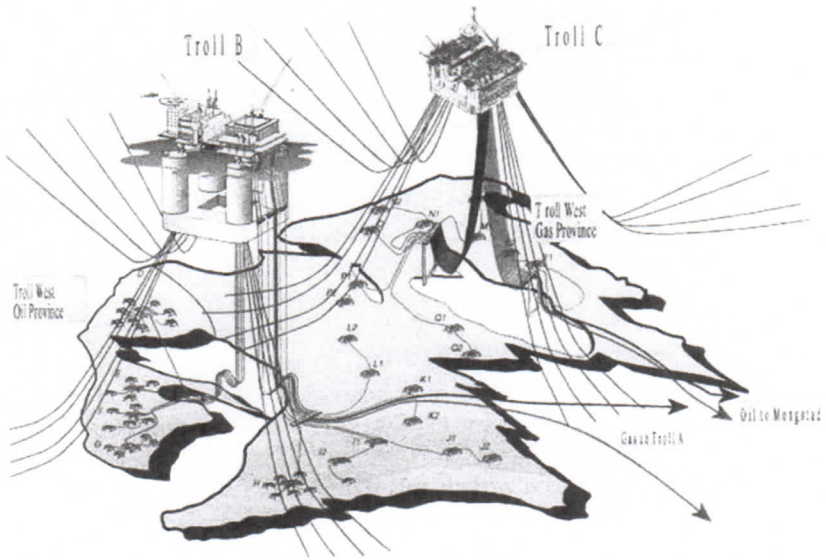

Figure 16 A schematic view of the Troll West Gas Province (TWGP) (after http://www.offshore-technology.com/projects/troll/).

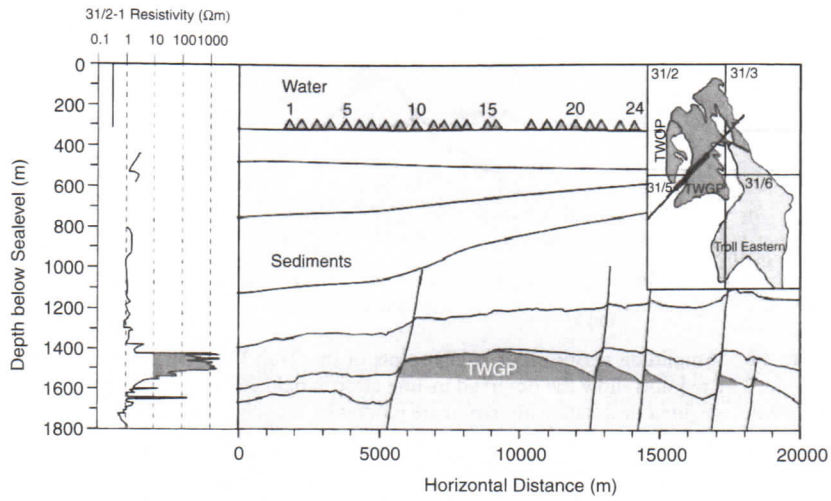

Figure 17 A simplified geological model along the MCSEM survey line in the Troll West Gas Province (TWGP), offshore Norway (after Johansen et al. (2005)).

transmitter was a horizontal electric bipole (HEB) with a length of 230 m towed by the survey vessel. The transmitting bipole generated a sine wave signal with a base frequency 0.25 Hz. The peak-to-peak current varied from zero up to 1000 amperes. The height of the towed transmitter was kept at a level of 40 m above the seafloor by an umbilical cable connected to the survey vessel. The observed EM data were measured in the time domain. These data were numerically transformed into the frequency domain and recorded as amplitudes and phases versus source-receiver offset curves. According to Johansen et al. (2005), the data quality is reliable with the source-receiver offset up to 8 km. Figure 17 shows a simplified geological model along the MCSEM survey line in the Troll West Gas Province (TWGP), offshore Norway (Johansen et al., 2005).

We should note that there are several publications dedicated to the inversion of the Troll MCSEM data (Chen et al., 2004; Hoversten et al., 2006; Gribenko and Zhdanov, 2007, etc.). In the paper by Hoversten et al. (2006), the finite difference-based inversion was used, while Gribenko and Zhdanov (2007), applied a rigorous inversion based on integral equation (IE) forward modeling.

In order to apply the migration algorithm developed in this paper to the Troll MCSEM data, we have selected a 1D layered background structure based on the 1D inversion (with a known water depth equal to 338 m). As a result of 1D inversion, the following parameters of the horizontally layered geoelectrical structure were obtained: the water conductivity is equal to 3 S/m and the conductivity of the sea-bottom sediment is 0.42 S/m.

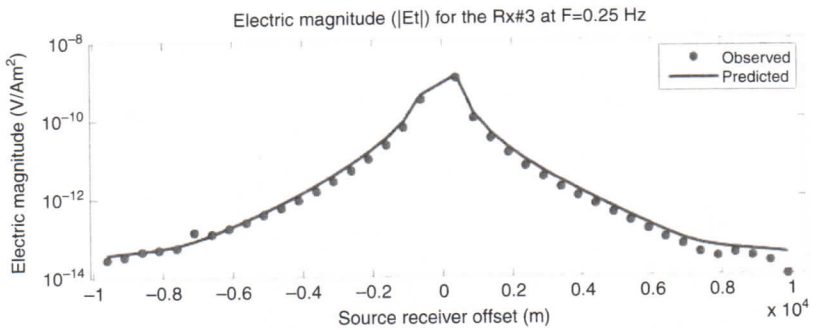

Figure 18 Amplitude versus offset (AVO) plots of the Troll Field data at a frequency of 0.25 Hz. The red dots show the observed in-line electric field data, while the predicted data for a model obtained by iterative migration are plotted by the solid blue line.

We have used this two-layer model as a background geoelectrical structure in our imaging and regularized iterative migration.

We have selected a domain of migration 21 km and 9 km long in the x- and y-directions, respectively, and 1.5 km deep in the vertical (z) direction from 400 m down to 1900 m below sea level, where the x axis of the Cartesian coordinates is oriented along the MCSEM profile, and the z axis is directed downward. This migration domain is discretized in $84 \times 18 \times 60 = 90,720$ cells, with the cell sizes 250, 500, and 25 m in the x, y and z directions, respectively, as shown in Figure 17. With previous knowledge of the seismic profile we designed an a priori model with the top layer in the x-direction being the seismic lines that mark the top of the reservoir in Figure 17 and the bottom at 1575 m with a resistivity of 3 Ohm m. We ran 70 iterations of migration. Note that the a priori model was applied only on the first 10 iterations and was switched off during the subsequent focusing.

The transmitters are located every 500 m along the transmitter line with a maximum offset equal to 10 km. We have used the data with the minimum offset of 500 m. Altogether, we used 24 transmitter locations for every receiver. In order to minimize the computational costs only the lower frequency of 0.25 Hz was selected. At the same time the EM field at this frequency penetrates deep enough in the conductive sediments to provide a clear response for the resistive reservoir. Amplitude versus offset (AVO) plots of the Troll Field data at a frequency 0.25 Hz are shown in Figure 18. The red dots show the observed in-line electric field data, while the predicted data for a model obtained by iterative migration are plotted by the solid blue line.

Figure 19 represents a 3D holographic image of the geoelectrical model obtained by migration imaging. Figure 20 represents overlapping of migration results with the geological interpreted section. One can see good agreement between the migration results and the geological section. The

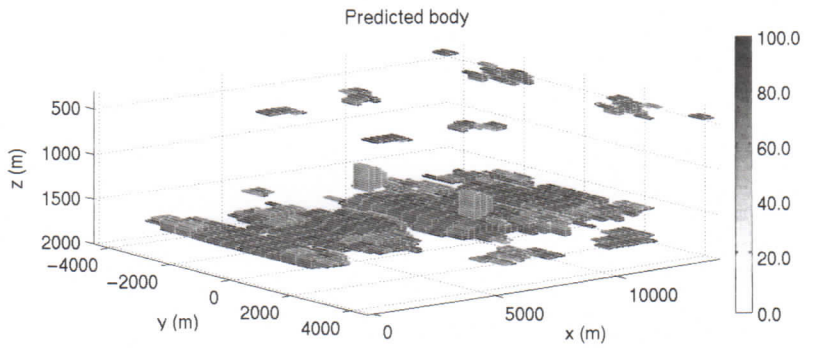

Figure 19 A 3D holographic image of Troll West Gas Province (TWGP), North Sea, obtained by iterative migration. The domains colored in blue show the migration image with the predicted resistivity above 50 Ohm m.

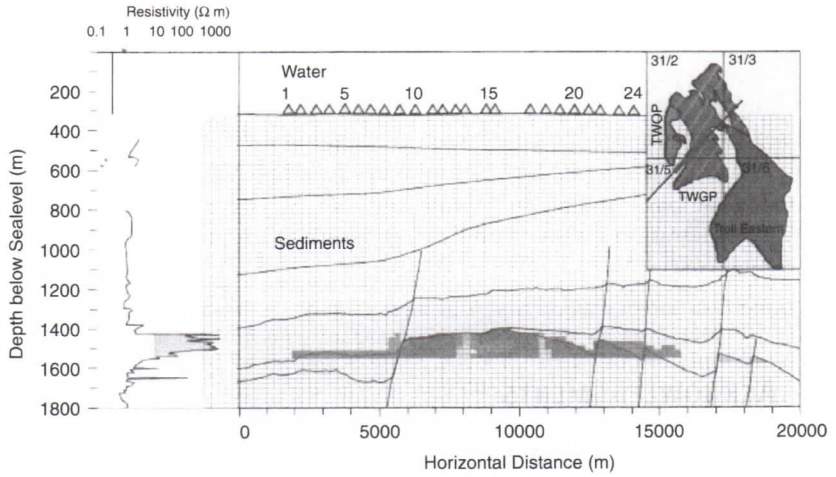

Figure 20 A cross section of the result of iterative migration overlapping on the geological cross section. The blue area overlapped with the geological section shows the migration image with the predicted resistivity above 20 Ohm m.

holographic/migration imaging method, which has been developed in this paper, has the ability to detect a strong resistivity anomaly in the area of the Jurassic sandstone reservoir.

8. Conclusion

Electromagnetic holography/migration was originally introduced for interpretation of land EM data. However, this technique is most effective

in the case of relatively dense EM surveys, which are difficult to implement on land. The MCSEM surveys with their dense system of transmitters and receivers happen to be extremely well suited to application of the EM holography/migration technique. In this paper we illustrate all the basic principles of EM holography/migration in application to MCSEM data interpretation. We show that, by using the reciprocity principle, we can represent the system of moving transmitters and fixed sea-bottom receivers by a survey with fixed sea-bottom transmitters and multiple seawater receivers. The migration (backscattering) field is produced by a combination of all electric dipole transmitters operating simultaneously according to the recorded signal in the receivers. The cross-power spectra of the migration and background electric fields generate a volume image of the anomalous conductivity distribution in sea-bottom formations.

In order to improve the resolution and quality of the migration image, we applied an iterative migration by repetitive backscattering of the residual field within the background medium. The backscattered field was computed using an IE based parallel computer code.

The basic principles of the migration imaging formulated in this paper were implemented in the computer code and are tested on a typical model of a sea-bottom petroleum reservoir. The holographic/migration imaging method was applied to interpretation of the practical MCSEM data acquired at Troll West Gas Province by Statoil and EMGS. The interpretation results show that migration can be treated as a prospective method of MCSEM data interpretation.

ACKNOWLEDGMENTS

The authors acknowledge the support of the University of Utah Consortium for Electromagnetic Modeling and Inversion (CEMI), which includes BAE Systems, Baker Atlas Logging Services, BGP China National Petroleum Corporation, BHP Billiton World Exploration Inc., British Petroleum, Centre for Integrated Petroleum Research, EMGS, ENI S.p.A., ExxonMobil Upstream Research Company, INCO Exploration, Information Systems Laboratories, MTEM, Newmont Mining Co., Norsk Hydro, OHM, Petrobras, Rio Tinto - Kennecott, Rocksource, Russian Research Center Kurchatov Institute, Schlumberger, Shell International Exploration and Production Inc., Statoil, Sumitomo Metal Mining Co., and Zonge Engineering and Research Organization.

We are thankful to Dr. Jonny Hesthammer and Rocksource for stimulating this research and fruitful discussions.

The authors thank Dr. Jens Danielsen of EMGS and Dr. Tage Røsten of StatoilHydro, and the Troll license group consisting of StatoilHydro, Petoro,

Norske Shell, Total, and ConocoPhillips, for providing the TWGP SBL data and permission to publish the result.

REFERENCES

Berdichevsky, M.N., Zhdanova, O.N., Zhdanov, M.S., 1989. Marine Deep Geoelectricity. Nauka, Moscow, 90 pp.

Chave, A.D., Constable, S.C., Edwards, R.N., 1991. Electrical exploration methods for the seafloor. In: Nabighian, M.N., Corbett, J.D. (Eds.), Electromagnetic methods in applied geophysics. In: Applications: Society of Exploration Geophysicists, vol. 2. Tulsa, Oklahoma, pp. 931–966.

Chen, J., Hoversten, G.M., Vasco, D.W., Rubin, Y., Hou, Z., 2004. Joint inversion of seismic AVO and EM data for gas saturation estimation using a sampling-based stochastic mode: Presented at the 74th Annual International Meeting, SEG.

Constable, S., Cox, C., 1996. Marine controlled source electromagnetic sounding - ii. The PEGASUS experiment: Journal of Geophysical Research 97, 5519–5530.

Evans, R.L., Sinha, M.C., Constable, S., Unsworth, M.J., 1994. On the electrical nature of the axial melt zone at 13 on the East Pacific Rise. Journal of Geophysical Research 99, 577–588.

Gribenko, A., Zhdanov, M.S., 2007. Rigorous 3D inversion of marine CSEM data based on the integral equation method. Geophysics 72 (2), WA73–WA84.

Johansen, S.E., Amundsen, H.E.F., Rosten, T., Ellingsrud, S., Eidesmo, T., Bhuyian, A.H., 2005. Subsurface hydrocarbons detected by electromagnetic sounding. First Break 23 (3), 31–36.

Hoversten, G.M., Cassassuce, F., Gasperikova, E., Newman, G.A., Chen, J., Rubin, Y., Hou, Z., Vasco, D., 2006. Direct reservoir parameter estimation using joint inversion of marine seismic and CSEM data. Geophysics 71, C1–C13.

MacGregor, L.M., Sinha, M.C., 2000. Use of marine controlled source electromagnetic sounding for sub-basalt exploration. Geophysical Prospecting 48, 1091–1106.

MacGregor, L.M., Sinha, M.C., Constable, S., 2001. Electrical resistivity structure of the Valu Fa Ridge, Lau basin, from marine controlled source electromagnetic sounding. Geophysical Journal International 146, 217–236.

Mittet, R., Maao, F., Aakervik, O.M., Ellingsrud, S., 2005. A two-step approach to depth migration of low frequency electromagnetic data: Presented at the 75th Annual International Meeting, SEG.

Novysh, V.V., Fonarev, G.A., 1966. Some results of the electrimagnetic study in the Arctic ocean. Geomagnetism and Aeronomy 6 (2), 406–409.

Portniaguine, O., Zhdanov, M.S., 1999. Focusing geophysical inversion images. Geophysics 64, 874–887.

Sinha, M.C., Patel, P.D., Unsworth, M.J., Owen, T.R.E., MacCormack, M.G.R., 1990. An active source electromagnetic sounding system for marine use. Marine Geophysical Research 12, 29–68.

Srnka, L.J., Carazzone, J.J., Ephron, M.S., Eriksen, E.A., 2006. Remote reservoir resistivity mapping. The Leading Edge 25, 972–975.

Trophimov, I.L., Fonarev, G.A., 1972. Some results of the magnetotelluric profiling in the Arctic ocean. Izvestia USSR Academy of Sciences 2, 81–92.

Tompkins, M.J., 2004. Marine controlled-source electromagnetic imaging for hydrocarbon exploration: interpreting subsurface electrical properties. First Break 22 (8), 27–33.

Wan, L., Zhdanov, M.S., 2005a. Rapid seabed imaging by frequency domain electromagnetic migration: Proceedings of Annual Meeting of the Consortium for Electromagnetic Modeling and Inversion, 169–186.

Wan, L., Zhdanov, M.S., 2005b. Rapid seabed imaging by frequency domain electromagnetic migration. Presented at the 75th Annual International Meeting, SEG.

Yoshioka, K., Zhdanov, M.S., 2005. Electromagnetic forward modeling based on the integral equation method using parallel computers: 74th Annual International Meeting, SEG, Expanded Abstracts.

Young, P.D., Cox, C.S., 1981. Electromagnetic active source sounding near the East Pacific Rise. Geophysical Research Letters 8, 1043–1046.

Zhdanov, M.S., 1981. Continuation of nonstationary electromagnetic fields in geoelectrical problems. Izvestia Akademii Nauk SSSR, Fizika Zemly 12, 60–69.

Zhdanov, M.S., 1988. Integral Transforms in Geophysics. Springer-Verlag.

Zhdanov, M.S., Frenkel, M.A., 1983a. The solution of the inverse problems on the basis of the analytical continuation of the transient electromagnetic field in reverse time. Journal of Geomagnetism and Geoelectricity 35, 747–765.

Zhdanov, M.S., Frenkel, M.A., 1983b. Electromagnetic migration. In: Hjelt, S.E. (Ed.), The Development of the Deep Geoelectric Model of the Baltic Shield, Part 2. Univ. of Oulu, Oulu, pp. 37–58.

Zhdanov, M.S., Keller, G., 1994. The Geoelectrical Methods in Geophysical Exploration. Elsevier, p. 873.

Zhdanov, M.S., Traynin, P., Booker, J., 1996. Underground imaging by frequency domain electromagnetic migration. Geophysics 61, 666–682.

Zhdanov, M.S., Traynin, P., 1997. Migration versus inversion in electromagnetic imaging technique. Journal of Geomagnetism and Geoelectricity 49, 1415–1437.

Zhdanov, M.S., 1999. Electromagnetic migration. In: Deep Electromagnetic Exploration. Springer-Verlag, Narosa Publishing House, New Delhi, pp. 283–298.

Zhdanov, M.S., 2001. Method of broad band electromagnetic holographic imaging: US Patent # 6,253,100 B1.

Zhdanov, M.S., 2002. Geophysical Inverse Theory and Regularization Problems. Elsevier, p. 609.

Zhdanov, M.S., Ueda, T., Gribenko, A., 2006. Iterative migration in marine CSEM data interpretation. In: Proceedings of Annual Meeting of the Consortium for Electromagnetic Modeling and Inversion, pp. 181–202.